Changes in the Biomechanical Response of the Optic Nerve Head in Early Experimental Glaucoma

Michael D. Roberts,[1] *Ian A. Sigal,*[1] *Yi Liang,*[1] *Claude F. Burgoyne,*[2] *and J. Crawford Downs*[1]

Purpose. To investigate the biomechanical response of the optic nerve head (ONH) connective tissues to IOP elevation in three pairs of monkey eyes in which one eye had early experimental glaucoma (EG).

Methods. A serial imaging technique was used to reconstruct the ONH and peripapillary sclera of three pairs of unilateral EG eyes fixed at 10 mm Hg. Eye-specific finite element models of the posterior pole were constructed with inhomogeneous material properties defined for the lamina cribrosa (LC) based on local connective tissue volume fraction (CTVF) and predominant LC beam orientation. These models were used to simulate an IOP increase from 10 to 45 mm Hg. A laminar material constant was varied to produce a range of LC displacements and scleral canal expansions, and the associated LC stress and strain were characterized.

Results. The models suggest that the LC of normal and EG eyes can deform posteriorly or anteriorly when the LC material stiffness is low or high, respectively. Scleral canal expansion was generally, but not always, reduced in EG eyes. Strains in the EG eye were similar to or lower than those in the contralateral eye for the same average LC displacement and increased when the LC was more pliant. Laminar stresses were consistently lower in the EG eye, regardless of LC stiffness.

Conclusions. Connective tissue remodeling in EG alters the biomechanical response of the LC to IOP elevation in an eye-specific manner. The models indicated that the LC tissues in EG eyes were more plaint than those in the contralateral normal eyes in two of three monkeys. (*Invest Ophthalmol Vis Sci.* 2010;51:5675–5684) DOI:10.1167/iovs.10-5411

Glaucoma is a progressive degenerative disease of the eye that, among its other effects, results in extensive alterations of the connective tissues in and around the optic nerve head (ONH). In the advanced stages of glaucoma, the connective tissues of the lamina cribrosa (LC) become posteriorly displaced and excavated beneath Bruch's membrane opening (clinical "cupping"), and the laminar beam network appears compressed or collapsed.[1] This change in laminar connective tissue anatomy represents a long-term remodeling process mediated by astrocytes and LC cells[2–4] that can compromise axonal function and may result in blindness. Although there is still debate as to whether this remodeling process is driven by mechanical, vascular, or other factors,[5,6] it is generally acknowledged that intraocular pressure (IOP) plays a central role in the disease.[7–11]

Various experimental animal models based on IOP elevation have been developed in attempts to better understand the tissue changes that underlie glaucoma. Of these, the monkey model of glaucoma is most used in studies of the ONH connective tissue, because the monkey has a highly developed LC that undergoes morphologic changes that are very similar to those in human glaucoma.[1] Prior work with this model has shown that connective tissue changes begin very early, only weeks after the induction of sustained elevated IOP. Specifically, these changes include posterior migration of the LC surface, thickening of the LC (possibly through recruitment of the immediate retrolaminar septa into the three-dimensional [3-D] LC structure[12]), expansion of the scleral canal, and a marked increase in the amount of connective tissue comprising the lamina.[12,13] Two of the changes that occur very early in the disease process—thickening of the LC and increase in total LC connective tissue volume—seem at odds with the longer term remodeling configuration associated with end-stage glaucoma and most likely represent a transient phase of disease progression. As such, they may provide important clues regarding the initiating events in this long-term remodeling process that eventually results in vision loss.

In recent years we have proposed a biomechanical paradigm for glaucoma that integrates mechanical, vascular, and cellular influences to describe the multiple changes that occur over a lifetime within the optic nerve head (ONH) during health and disease.[5,14,15] Within this paradigm, we hypothesize that IOP-related stresses and strains within the load-bearing connective tissues of the ONH play a key role in modulating local blood flow, diffusion processes, and cellular activity, such that a state of mechanical and biological homeostasis is maintained. As such, the mechanical and vascular hypotheses of glaucomatous damage become complementary rather than dichotomous, and the dynamics of the entire system as a mechanobiological entity are highlighted.

We have described techniques for characterizing the microarchitecture of the LC[12] and how this information can be used to computationally model the mechanical environment within the LC and peripapillary sclera by using finite element modeling.[16] In the present study, we applied the same techniques to model the biomechanical response of three pairs of monkey eyes with unilateral early experimental glaucoma (EG) to acute IOP elevation. Because of the aforementioned changes in anatomy and microarchitecture of the ONH connective tissues that occur in EG, it is important to understand the concomitant changes in the IOP-related displacements, stresses, and strains that take place in these

From the [1]Ocular Biomechanics and [2]Optic Nerve Head Research Laboratories of the Devers Eye Institute, Legacy Health System, Portland, Oregon.

Supported in part by USPHS Grants R01EY011610 (CFB) from the National Eye Institute, National Institutes of Health, Bethesda, MD, and the Legacy Good Samaritan Foundation, Portland, OR

Submitted for publication February 19, 2010; revised April 22, 2010; accepted May 14, 2010.

Disclosure: **M.D. Roberts**, None; **I.A. Sigal**, None; **Y. Liang**, None; **C.F. Burgoyne**, None; **J.C. Downs**, None

Corresponding author: J. Crawford Downs, Ocular Biomechanics Laboratory, Devers Eye Institute, 1225 NE 2nd Avenue, Portland OR 97232; cdowns@deverseye.org.

remodeled EG eyes compared with those in their contralateral normal controls.

However, our modeling techniques require target deformations for each model that are ideally based on experimental data. Although there are numerous studies on IOP-related deformation of the ONH surface, there are no published data on in vivo ONH connective tissue mechanical deformation. Recent experimental data derived by using a postmortem, 3-D histomorphometric technique suggest that the LC of normal eyes can move either posteriorly or anteriorly, depending on eye-specific geometric and material property factors, and that the magnitude of this displacement is small (approximately ± 7 μm).[17] In EG eyes, however, determination of the LC displacement by such 3-D histomorphometric approaches is problematic because it is unclear how to separate the laminar deformation into its permanent (remodeled) and acute (mechanical) IOP-related components (Burgoyne CF, et al. *IOVS* 2010;51: ARVO E-Abstract 2137). In light of this uncertainty, in the present study we varied the LC material stiffness of each EG and contralateral normal eye to produce a wide range of target LC displacements, both posterior and anterior, and characterized the concomitant changes in scleral canal expansion, and stress and strain in the LC for IOP increase from 10 to 45 mm Hg.

Materials and Methods

The strategy used in this study to examine the biomechanical response of eye pairs to elevated IOP was similar to that used in a previous study of the IOP response of bilaterally normal eyes.[16] Briefly, in the present study, we constructed eye-specific finite element models of eye pairs from three monkeys with unilateral EG, and simulated each eye's biomechanical response to an acute IOP elevation from 10 to 45 mm Hg, to assess the effect of early glaucoma on ONH biomechanics. This response was characterized in terms of anterior LC surface displacement, scleral canal expansion, and stress and strain within the LC. Since it was necessary to estimate a laminar material constant, A, which is proportional to the material stiffness of the lamina but has yet to be characterized experimentally, we also evaluated the effect of this parameter on model behavior. As in our previous study, this laminar stiffness constant was varied to simulate LC material properties ranging from pliant to stiff. All other model parameters, including the scleral elastic modulus, scleral shell geometry, and the eye-specific LC anisotropy and inhomogeneity, were held constant within each eye-specific model.

Animals

Three male cynomolgus monkeys, approximately 8 years of age, were used (see Table 1 of Ref. 18 for details). Analyses of the ONH anatomy and LC microarchitecture of these animals have been presented in two previous reports.[12,13] All animals were treated in accordance with the ARVO Statement for the Use of Animals in Ophthalmic and Vision Research.

Table 1 summarizes several of the baseline (IOP = 10 mm Hg) characteristics of these eyes that are relevant to the present modeling approach. At the top of this table, nasotemporal cross sections through the central portion of the reconstructed geometry are depicted (reconstruction details will be provided later). The bottom portion of the table is a compilation of information on average laminar position (an indication of LC cup depth), laminar and peripapillary thickness,[12] LC connective tissue volume fraction,[13] and total LC connective tissue volume.

Early Experimental Glaucoma

The creation of early experimental glaucoma in one eye of each monkey has been characterized in our previous reports.[13,18–20] Briefly, photocoagulation of the trabecular meshwork was performed on one eye to induce chronic but moderate IOP elevation. Early glaucoma was defined in these eyes as the earliest change in ONH surface position, as measured by confocal scanning laser tomography (CSLT). The duration and magnitude of moderate IOP elevations in each monkey were as follows: monkey 1 was killed at 6 weeks and monkeys 2 and 3 at 3 weeks after CSLT confirmation of ONH surface change. In monkeys 1 and 2, IOP elevations were moderate with only one measurement higher than 30 mm Hg. In monkey 3, elevated IOP was not detected, although there was confirmed ONH surface change (Table 1, Fig. 1 of our previous publication[18]). Significant axonal loss in the EG eyes was an average of 16%, 30%, and 19% in monkeys 1, 2, and 3, respectively.[20] Note that all eyes in the study were perfusion fixed with the IOP set at 10 mm Hg in both eyes at death.

3-D Reconstruction and Delineation of ONH and Peripapillary Sclera

Paraffin-embedded tissue samples of the ONH and peripapillary sclera were 3-D reconstructed with a serial sectioning technique described previously.[18] Custom software was used to delineate boundaries corresponding to the neural canal wall and the anterior and posterior surfaces of the LC and peripapillary sclera. These delineated tissue boundaries were interpolated to generate the outer surfaces of a closed LC region within which a custom volumetric segmentation algorithm was used to classify voxels as either connective or nonconnective tissue.[12,21]

Finite Element Modeling

Finite element (FE) models were generated using the same procedure as previously described for models of bilaterally normal monkey eyes.[16] Briefly, the user-delineated 3-D surfaces were incorporated into a generic scleral shell of the posterior pole with anatomic thickness variations mapped from previous histologic studies.[22,23] The LC–scleral shell complex was used to define the geometry for a finite element model using a commercial finite element pre- and postprocessing system (Patran, Santa Ana, CA). Quadratic hexahedral finite elements were used for all FE calculations. The nodes along the equatorial sclera were constrained to allow radial movement only. A pressure load of 35 mm Hg was applied to the interior surface of the model to simulate an IOP increase from 10 to 45 mm Hg. Analyses were performed with a commercial finite element analysis code (Abaqus ver; 6.1; Dassault Systèmes Simulia Corp., Providence, RI), using finite deformation theory with Cauchy true stress and logarithmic strain calculated in the models.

As with the previous studies, the FE models included the LC and sclera tissues of the posterior pole, but did not include the prelaminar neural tissues, the pia mater, or the retrolaminar optic nerve. The sclera modulus was derived from the equilibrium modulus found in uniaxial stress relaxation tests of normal and EG monkey eyes (4.94 and 7.46 MPa, respectively)[24,25] and was assigned to the model as a homogeneous, linear, isotropic material. As described in our previous report,[16] this scleral elastic modulus was scaled up by a constant factor to offset the scaling down of scleral thickness map values that was necessary to smoothly incorporate the 3-D reconstruction into the generic scleral shell with minimal discontinuity. The intended effect of this modulus scaling procedure was to preserve structural stiffness so that the scleral shells of each of the FE models would resist IOP loading similarly and transmit hoop stress to the peripapillary sclera and LC in a consistent manner.

Unique orthotropic material properties were assigned to each finite element in the LC based on local connective tissue volume fraction and fabric (predominant beam orientation) along with a global laminar material constant, A, as previously described.[12,16]

Output Measures of Mechanical Response

The biomechanical response for each model was characterized in terms of anterior LC surface displacement, scleral canal expansion at

TABLE 1. Geometric and Microarchitectural Characteristics of Each Pair of Eyes Fixed at IOP of 10 mm Hg, Representing the Baseline Configurations from Which Finite Element Models Were Constructed

Structure	Monkey 1		Monkey 2		Monkey 3	
	N	EG	N	EG	N	EG
Laminar position, μm	−102	−220*	−111	−208*	−105	−184*
Laminar thickness, μm	103	164*	128	151*	83	109*
Peripapillary scleral thickness, μm	136	132	126	94*	113	114
Connective tissue volume fraction	0.33	0.26	0.32	0.33	0.33	0.31
Connective tissue volume, million μm^3	80	146*	61	88*	57	81*

A thick, cross-sectional view through the central nasotemporal portion of the LC is shown for each eye. Average LC position, LC thickness, and peripapillary thickness are taken from Table 2 of Reference 13. Connective tissue volume and volume fraction data were compiled from Reference 12.

* Significant difference versus contralateral normal 1.

FIGURE 1. IOP-induced LC displacement is calculated relative to the anterior laminar insertion, to remove the global displacement of the scleral shell. (**A**) The full finite element model displacement field for a 35-mm Hg IOP increase shows that the LC elements displace substantially and tilt relative to the scleral shell equator. Note that the titling occurs because the inferior LC displaces more than the superior LC due to nonuniform scleral displacements (as the scleral shell deforms it pulls the LC with it). (**B**) This superior–interior tilting is more apparent when the LC elements are plotted with a narrower range to focus on laminar displacement only. (**C**) LC displacement relative to the anterior laminar insertion displays the laminar deformation with the component of displacement removed. In this example, the central LC displaces posteriorly. Examples of anterior displacement of the central LC can be seen in Figure 2.

the anterior and posterior laminar insertions, and strain and stress within the LC.

LC position was determined by averaging the normal distances between a plane fit to the anterior laminar insertion and the nodes lying on the anterior LC surface. The difference in LC position between the unloaded and loaded states represents the LC displacement relative to the anterior laminar insertion and effectively removes the global tilting of the LC as it moves with the scleral shell during inflation. An example of this calculation of LC displacement is shown in Figure 1. Using this LC displacement metric, we were able to adjust the laminar material constant A to produce a range of average LC displacements for each eye-specific model.

Mean scleral canal expansion at the anterior laminar insertion was calculated by first determining the centroid of the scleral canal before and after IOP elevation by fitting a least-squares ellipse to the nodes on the anterior laminar insertion in the unloaded and loaded states. Anterior scleral canal expansion was defined as the average IOP-induced change in distance from the centroid to each of the anterior laminar insertion nodes. A similar calculation was performed for the nodes of the posterior laminar insertion to quantify IOP-induced posterior scleral canal expansion.

Strain and stress within the LC region of the models were characterized by calculating the first principal strain (i.e., tensile strain) and von Mises stress within the LC and presenting contour plots associated with average LC displacements of −20, −5, and +5 μm (moving from posterior to anterior, with corresponding laminar material properties ranging from plaint to stiff). For each LC pair, an average strain (or

stress) value was calculated, and box plots were produced for a range of LC displacements ranging from −40 to +10 μm.

Overall Differences in FE Model Output Parameters between Normal and EG Eye Pairs

To distill the differences in mechanical response between normal and EG eyes into a more accessible form, we tabulated the aforementioned output measures as follows: the normal eye was assumed to have negligible LC displacement in accordance with recent data from our laboratory and others[17] (Agoumi Y, et al. *IOVS* 2009;50:ARVO E-Abstract 4898) (i.e., its laminar material constant was adjusted to produce 0 LC displacement). The EG eyes were considered to have acute LC displacements ranging from −40 to +10 μm (posterior [outward] to anterior [inward], respectively). Average values for the anterior and posterior scleral canal expansion, maximum principal strain, the von Mises stress, and the associated laminar material constant were tabulated.

Results

Predicted Laminar Displacement

The LC displacement relative to the anterior laminar insertion for normal and EG eye pairs in each of the three monkeys is shown in Figure 2. In all cases, as the LC stiffnesses changed from plaint to stiff, the average LC displacement transitions from a large posterior bulging of the central lamina to a small anterior LC deformation concentrated along the superior-inferior axis (Fig. 2). In all eyes, the models with a high laminar material constant (and hence a stiff LC) were able to produce an average anterior LC displacement of at least +5 μm or more. Of interest, the deformation for these stiff cases was nonuniform and saddlelike, with the superior and inferior regions displacing anteriorly, and the nasal and temporal regions displacing posteriorly. Generally, the LC deformation plots show a high degree of similarity both within eye pairs and across animals. Note that the LC deformation plots in Figure 2 correspond to model simulations with laminar material constants adjusted to produce equal amounts of average LC displacement, and the laminar material constant required to produce each of these LC responses can be determined from the graphs at the bottom of the same figure.

The propensity for anterior displacement of the LC surface was greater in the EG eyes of monkeys 2 and 3 than in their contralateral normal eyes, as demonstrated by the separation of the mean LC displacement curves for the normal and EG eyes in the lower panels of Figure 2. In monkey 1, the LC displacement behavior of the normal and EG eyes were remarkably similar (both in the deformation plots and the mean LC displacement curves) despite the extensive connective tissue remodeling in the EG eye that produced a thicker and more deeply cupped LC in this animal (see Table 1).

Predicted Scleral Canal Expansion

In each model, posterior scleral canal expansion was generally greater than anterior scleral canal expansion, particularly at low to medium values of the laminar material constant (Fig. 3). At large values of the laminar material constant, the scleral canal expansion curves of the EG eyes for monkeys 2 and 3 crossed, indicating that it is possible for anterior scleral canal expansion to exceed posterior scleral canal expansion in the models when the LC is sufficiently stiff. In monkeys 1 and 3, scleral canal expansions in the EG eye were less than the corresponding curves for their contralateral normal eyes. In monkey 2, the scleral canal expansion curves of the EG eye were bounded by the anterior and posterior expansion curves of the contralateral normal. For the range of laminar stiffness constants considered (plaint to stiff), the normal anterior and posterior scleral canal expansions ranged from 32 to 17 μm and from 35 to 20 μm, respectively. In the EG eyes, anterior and posterior scleral canal expansions ranged from 23 to 13 μm and from 24 to 14 μm, respectively.

In Table 2, anterior and posterior scleral canal expansion data were compiled for the case in which the laminar material constant was adjusted to produce 0 LC displacement in the normal eye and a range of LC displacement responses for the

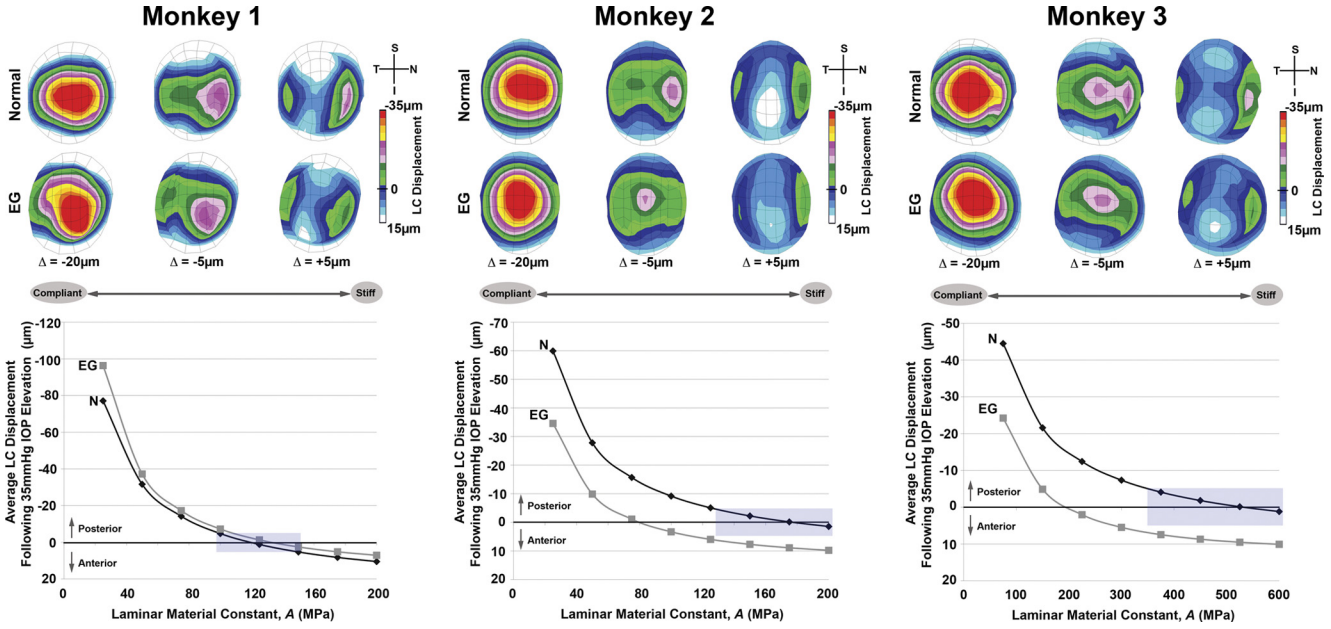

Figure 2. LC displacement of paired normal and EG eyes of each monkey as a function of laminar stiffness. Note that in all eyes, when the laminar material constant, *A*, was low (i.e., a plaint LC) the central portion of the LC bulged posteriorly, and the average laminar displacement was large. When the laminar material constant was large (i.e., a stiff LC), the superior–inferior axis of the LC exhibited small anterior displacements. The highlighted region denotes the laminar material constant range over which average LC displacement is −5 to +5 μm.

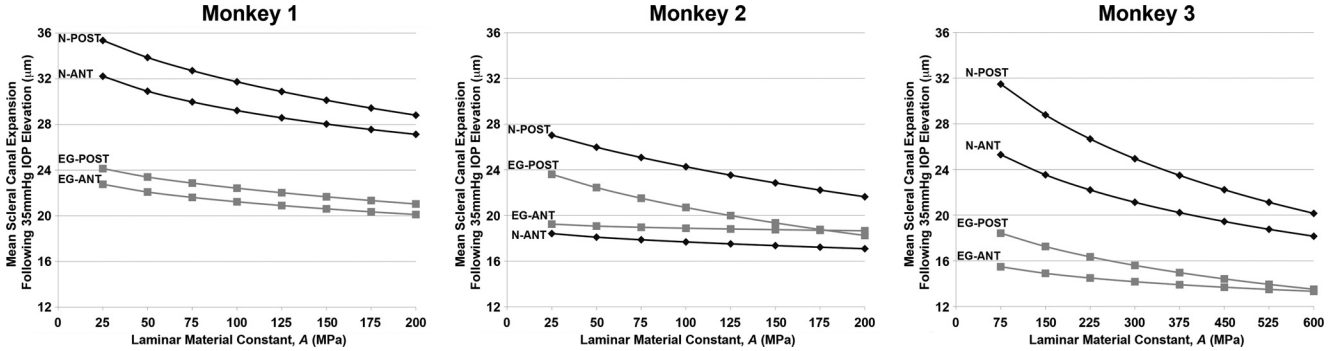

FIGURE 3. Anterior and posterior scleral canal expansion in paired normal and EG eyes of each monkey as a function of laminar stiffness. These plots show that anterior and posterior scleral canal expansion was not as strongly affected by the laminar stiffness as LC displacement and was on the order of 3% to 4% of the scleral canal radius at IOP 10 mm Hg. These data also suggest that posterior scleral canal expansion within a given eye was generally larger than anterior scleral canal expansion, with the EG eye of monkeys 2 and 3 being an exception at high values of the laminar material constant. Note that both anterior and posterior canal expansion were lower in the EG eye than in the normal eye in monkeys 1 and 3, which is likely a reflection of the higher scleral modulus of elasticity assigned to the EG eye models. This clear separation between normal and EG canal expansion was not present in monkey 2, which had a significantly thinner peripapillary sclera.

EG eye. As can be deduced from the curves of Figure 3, scleral canal expansion of the normal eye of monkeys 1 and 3 always exceeded that of the EG eye, both anteriorly and posteriorly, regardless the LC displacement and corresponding LC stiffness of the EG eye. For monkey 2, however, anterior scleral canal expansion is consistently, but only slightly, larger in the EG eye than in the normal eye. This pattern is reflected in both the curves of Figure 3 and the data of Table 2. Posterior scleral canal expansion of the EG eye can exceed that seen in the reference normal case (i.e., when the normal eye undergoes 0 net LC displacement at $A = 177$ MPa) when the EG eye is highly plaint ($A < 50$ MPa), but this behavior is reversed as the EG laminar material constant increases. An explanation of the seemingly anomalous scleral canal expansion behavior of monkey 2 is provided in the Discussion section.

Predicted Laminar Strain and Stress

In Figure 4 the maximum principal strain (i.e., the most tensile principal strain) in the LC is characterized for each pair of eyes as a function of LC displacements over a range of -40 μm (posterior) to $+10$ μm (anterior). As depicted for each pair, the LC strain magnitudes were similar between normal and EG eyes for a given average LC displacement, with the more plaint

TABLE 2. Comparison of Biomechanical Response of a Normal Eye with 0 Average LC Displacement with an Early EG Eye at Various Levels of Average LC Displacement

	LC Displacement (μm)					
	Normal Eye	Early EG Eye				
	0	−40	−20	−10	0	10
Monkey 1						
Laminar material constant *A,* MPa	119	48	70	92	133	264
Ant. scleral canal expansion, μm	28.7	22.1	21.7	21.4	20.8	19.6
Post. scleral canal expansion, μm	31.1	23.5	23.0	22.6	21.9	20.4
Max. principal strain, %	1.1	1.9	1.3	1.0	0.8	0.5
Von Mises stress, MPa	11.6	4.3	4.6	4.9	5.6	7.5
Monkey 2						
Laminar material constant *A,* MPa	177	22	36	50	80	206
Ant. scleral canal expansion, μm	17.2	19.3	19.2	19.1	18.9	18.7
Post. scleral canal expansion, μm	22.2	23.8	23.1	22.5	21.3	18.1
Max. principal strain, %	0.9	1.8	1.3	1.0	0.8	0.6
Von Mises stress, MPa	12.6	3.7	4.1	4.5	5.5	9.2
Monkey 3						
Laminar material constant *A,* MPa	532	52	85	119	196	590
Ant. scleral canal expansion, μm	18.7	15.7	15.4	15.1	14.6	13.4
Post. scleral canal expansion, μm	21.0	18.9	18.2	17.7	16.7	13.6
Max. principal strain, %	0.8	1.4	1.0	0.8	0.6	0.4
Von Mises stress, MPa	40.0	6.6	7.5	8.5	10.4	18.0

Negative values apply to posterior and positive values to anterior LC displacement. Mean values are reported for anterior and posterior scleral canal expansions, maximum principal strain, and Von Mises stress. The reported laminar material constant represents the material stiffness value necessary to produce the associated average LC displacement in the table columns.

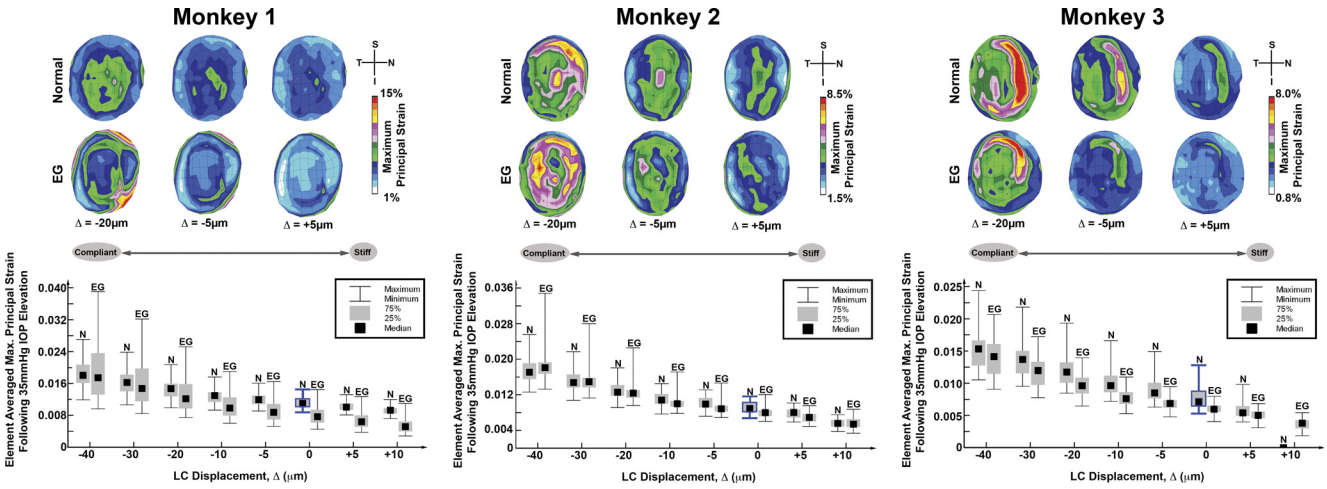

FIGURE 4. Maximum principal strains in the LC associated with different amounts of average LC displacement. *Top*: anterior surface view of the tensile strain for normal and EG eyes of each monkey for −20, −5, and +5 μm average LC displacement. *Bottom*: median-based box plots of elemental tensile strain in the lamina for target LC displacements ranging from −40 to +10 μm for both eyes of each monkey. These plots show that strains are higher in plaint versus stiff LCs. The similarity in strain distributions in paired normal and EG eyes at equivalent average LC displacement values is apparent. The box plot of strains in the normal eye with 0 average LC displacement is highlighted in *blue* to facilitate comparison to other box plots.

LCs having larger median and maximum/minimum values than the stiffer LCs. The regions of maximum strain occurred predominantly in the nasal or inferior regions of the LC, whereas the site of lowest strain was highly variable across all eyes.

In Table 2, we note that when the EG eye experienced an average posterior LC displacement of approximately −10 to −15 μm, the average strains were similar to those in the contralateral eye at an LC displacement of 0. At −20 and −40 μm of posterior LC displacement, the EG eye LC strains were much higher than in the normal eye at 0 LC displacement. On the other hand, EG eyes with 0 or anterior LC displacement had lower average tensile strains. For anterior LC displacement of +10 μm in the EG eye, strains were 52%, 38%, and 52% lower in monkeys 1, 2, and 3, respectively, compared with the contralateral normal eye with 0 average LC displacement.

Figure 5 shows von Mises stress plotted for laminar material constants ranging from plaint to stiff. These plots show that as LC displacement increases, the median and maximum/minimum stresses within the normal eyes increase much more dramatically and rapidly than in the EG eyes. In other words, for the same LC displacement, the normal LC is under greater mechanical stress than the contralateral EG eye. Stress tended to concentrate centrally and temporally in all eyes, and the lowest stresses were located superiorly and nasally. Table 2 indicates that average von Mises stress in the EG eye over the range of average LC displacement considered was consistently lower than the stress in the normal eyes with 0 net LC displacement. Over the range of EG displacements considered (−40 to +10 μm) percent reductions in average LC stress ranged from −63% to −36%, −70% to −26%, and −84% to −55%, in monkeys 1, 2, and 3, respectively.

DISCUSSION

In this article, we have reported biomechanical modeling results for three pairs of monkey eyes with unilateral early ex-

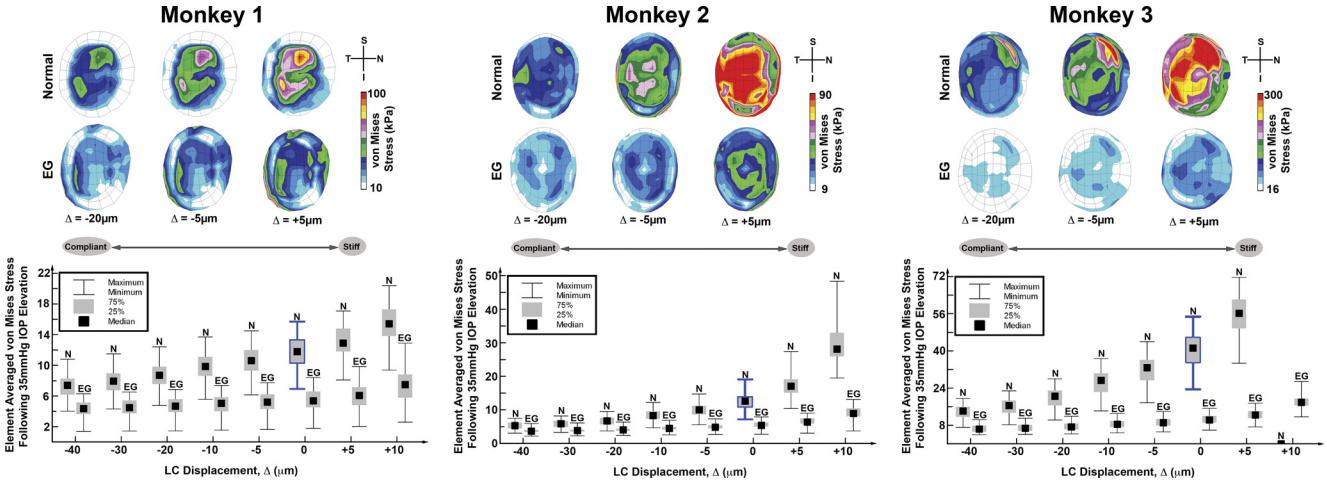

FIGURE 5. von Mises stress in the LC associated with different amounts of average LC displacement. *Top*: anterior surface view of the von Mises stress in the normal and EG eyes of each monkey for −20, −5, and +5 μm average LC displacement. *Bottom*: median-based box plots of elemental stress in the lamina for target LC displacements ranging from −40 to +10 μm for both eyes of each monkey. These plots show that as the LC was made stiffer and transitioned from a posterior to anterior displacement, the stresses in the normal eye were higher than in the contralateral EG eye and increased more quickly as a function of LC displacement. The box plot of stresses in the normal eye with 0 average LC displacement is highlighted in *blue* to facilitate comparison to other box plots.

perimental glaucoma. These finite element models include eye-specific variations in LC thickness, peripapillary sclera thickness, LC curvature, and also incorporate a description of the local laminar connective tissue microarchitecture into the mechanical properties of the LC.[12,16] As such, the models of the EG eyes reflect the remodeling–associated thickening and posterior cupping of the LC connective tissues that have been reported previously.[12,20] In our previous paper, we showed that normal monkey eye pairs exhibit very similar mechanical response to IOP elevation.[16]

The present models suggest that the LC of normal and EG eyes can deform posteriorly or slightly anteriorly when the LC material stiffness is low or high, respectively. Scleral canal expansion was generally, but not always, reduced in EG eyes. Strains in the EG eye were similar to or lower than those in the contralateral eye for the same average LC displacement and increased when the LC was more plaint. Laminar stresses were consistently lower in the EG eye, regardless of LC stiffness.

The capacity for the LC to displace in either the posterior or anterior direction for both normal and EG eyes is in agreement with previously reported biomechanical simulations of bilaterally normal monkey eyes[26] and models of reconstructed human eyes.[27,28] Moreover, such posterior and anterior displacement of the LC surface under acute IOP elevation has been demonstrated histologically in nonglaucomatous monkey eyes[17] and in vivo in human eyes (Agoumi Y, et al. *IOVS* 2009;50:ARVO E-Abstract 4898). Unfortunately, in vivo data on the LC response to acute IOP elevation for glaucomatous monkey eyes are sparse, and it has proven problematic to separate the IOP-induced acute deformations and permanent remodeling-induced deformations in a histologic analysis of these tissues (Yang Y, et al., manuscript submitted). In the absence of eye-specific data on the direction and magnitude of LC displacement, we acknowledge that specific statements about the altered biomechanical environment in EG described by computational models—particularly, the stress and strain environment—represent informed speculation. Thus, we reaffirm the importance of continued development of next-generation imaging devices and techniques to probe both the geometry of the deeper connective tissues of the ONH and their deformational response to elevated IOP. For instance, deep scanning SD-OCT may eventually offer a powerful new approach to track the remodeling-associated permanent posterior cupping of the LC surface over time, while also offering the possibility of measuring the acute LC deformation caused by an applied IOP increase during imaging[29–31] (Burgoyne CF, et al. *IOVS* 2007;48:ARVO E-Abstract 3296; Burgoyne CF, et al. *IOVS* 2010; 51:ARVO E-Abstract 2137). That said, the eye-specific models presented herein, considered in combination with experimental and computational studies of bilaterally normal eyes, suggest that EG does change the biomechanical response of the LC to acute IOP elevation.

In a similar vein, it is important to reiterate that although our FE models captured eye-specific geometric and microarchitectural characteristics, the scleral elastic modulus assigned to these models was not specific to each eye. Rather, scleral material properties were based on pooled uniaxial mechanical testing data from normal and EG scleral specimens from a separate group of eyes in which EG was found to increase the elastic modulus by 51%. More recent inflation testing of monkey posterior scleral shells has confirmed that the sclera is generally stiffer in monkeys with EG[32,33] and also in older monkeys.[34]

In the context of the present study, this introduction of stiffer EG scleral properties into FE simulations may have exerted a strong effect on our biomechanical outcome measures, particularly scleral canal expansion. Sigal et al.,[35] have shown that scleral modulus has a substantial influence on scleral canal expansion and our simulations capture this effect for monkeys 1 and 3 as a dramatic separation between the canal expansion curves for the normal and EG treatments (Fig. 3). In the case of monkey 2, where scleral canal expansions are more similar between the normal and EG eyes, we note that the EG eye of this animal was shown to have undergone marked and significant thinning of the peripapillary sclera (~25% as shown in Table 1),[13] a geometric feature that is captured in our FE model. This scleral thinning served to offset the stiffening effect of the increased scleral elastic modulus assigned to the EG eye such that the effective, or structural, stiffness of the peripapillary sclera was reduced more than in the other two EG eyes. Such interactions between material and geometric factors have recently been studied in depth by Sigal et al.[36] for stress and strain outcome measures, where it was shown that the influence of scleral stiffness can be modulated and even outweighed by other material and geometric factors. The effect of such factor interactions on deformation measures is studied in a separate report (Sigal IA et al., manuscript submitted).

The eye-specific changes in LC geometry engendered by progression from normal to EG should also be expected to alter the biomechanics of the LC, both in terms of laminar deformation and average LC displacement, and in terms of the strain and stress environment. In the case of LC displacement, we note that in two of the subjects (monkeys 2 and 3) the mean LC displacement versus laminar material constant curves of the EG eyes are shifted downward (i.e., anteriorly) relative to the contralateral normal curve. As a result, for the contralateral normal and EG eyes to be displaced by the same amount, the laminar material constant for the EG eye would have to be lower than in the contralateral normal eye (i.e., the LC in EG would have to have lower *material* stiffness). An alternative interpretation of these curves is that if the normal and EG eyes have similar laminar material constants (similar material stiffness), then the EG eye would have less posterior displacement or more anterior displacement for the same IOP increase (i.e., the LC would be *structurally* stiffer in the EG eye). For monkey 1, however, the LC displacement curves in the normal and EG eyes was remarkably similar (i.e., they overlap). This behavior is perhaps due to a compensatory effect of the large amount of connective tissue remodeling observed in this EG eye. As previously reported, the connective tissue volume increased substantially in this particular eye,[12] and this change manifests in the FE models as increased LC thickness, deeper cupping, and decreased CTVF, when compared with the changes seen in the EG eyes of monkeys 2 and 3 (see Table 1). These geometric and microarchitectural changes appear to combine to produce an LC that is effectively as stiff overall as its contralateral normal eye and hence deforms similarly as a function of the laminar material constant.

The previous two paragraphs highlight the importance of augmenting our present analysis approach based on detailed, eye-specific ONH 3-D reconstructions with imaging approaches to allow characterization of connective tissue deformation response to increased IOP. It is conceivable that such a capability combined with the present framework would allow us to estimate individual scleral elastic modulus from measurement of scleral canal expansion. Similarly, characterization of the acute IOP-induced displacement of the LC surface may provide insight into the relative stiffness or pliancy of the LC and surrounding peripapillary sclera in an individual. We believe that such an advance will be a critical component in the elucidation of ONH biomechanics in health, aging, and disease.

In anticipation of techniques that will allow LC response to acute IOP elevation to be directly measured, we have presented our strain and stress data plotted as a function of mean LC displacement (Figs. 4, 5, Table 2). For the strain data, if we again assume that the EG and contralateral normal eye deform

under IOP in a similar fashion, our simulations suggest that strains in the EG eye will be roughly the same or slightly lower than in the normal eye. More specifically, if we take as a point of reference that the mean LC displacement is small (±5 μm) in normal eyes (as observed in a 3-D histomorphometric analysis,[17] then the contralateral EG eye must displace posteriorly by approximately −20 μm or more in order for the median strains in the EG eye to exceed the median strain in the normal eye. Such a displacement would also require that the EG eye be much less materially stiff than its contralateral normal eye. This same interpretation is borne out by the data compiled into Table 2. Conversely, anterior LC displacement of the EG eye would serve to lower the strains in the LC tissue. Again, the data in Table 2 succinctly show this phenomenon.

The distinction between posterior and anterior LC displacement and its effect on strain increase or decrease could have important implications for the mechanobiology of the LC. Strain, because it quantifies the physical manifestation of tissue deformation under load, has been hypothesized to be a likely regulator mechanical adaptation in numerous tissue types.[14,37,38] In the lamina, evidence is mounting in support of astrocyte mechanosensitivity to strain[39–41] (Rogers R, et al. *IOVS* 2009;50:ARVO E-Abstract 888), which in turn may provide a feedback mechanism by which mechanical strain can influence connective tissue remodeling. Our simulations suggest that average LC displacement (both the magnitude and direction) may be useful as an indicator of changes in the connective tissue strain environment and therefore may correlate with astrocyte-mediated connective tissue remodeling in the ONH.

Stress was the biomechanical output measure that showed the largest and most consistent treatment effect in this study. In all three monkey eyes, the stress in the EG eyes was lower across all LC displacement values than in the contralateral normal eyes. We suspect that the explanation for this is twofold: First, scleral stiffening in EG may contribute to a stress-shielding phenomenon whereby increased load carried in the sclera diminished the load that is borne by the LC. Second, the increased thickness and curvature of the EG eye's LC combines in a manner that reduces the stress transmitted through LC. The combined effect of LC thickness and curvature on stress is well-illustrated in the normal LC of monkey 3, for example, where a very thin, flat LC resulted in higher stresses than in other eyes. Although strain is often considered the most relevant index of the biomechanical environment in mechanotransduction, there is still no firm consensus, and some have argued that stress may be an important driver of tissue remodeling and adaptation, since it reflects the level to which regions of tissue are engaged in load-bearing and transmission.[42] Our simulations suggest that the early connective tissue remodeling of EG results in a marked reduction of stress in the LC. As such, we believe that stress should still be considered an important metric in the biomechanical paradigm of glaucoma development and progression.

We have thoroughly discussed the limitations of our FE modeling approach in a previous report[16] and briefly present it here. To summarize, the sclera and LC are modeled using linear isotropic and linear orthotropic material properties, respectively, and prestress within the tissue is neglected, even though samples have been perfusion fixed at 10 mm Hg. The laminar microstructure-to-stiffness relationships used to assign laminar material properties have not been experimentally verified in LC tissue, but similar relationships have been adopted to model other anisotropic, trabecular-like structures.[43–46] Their use has been retained for the present models in the absence of full-field pressure-displacement data for the constitutive model development. It should also be noted that the calculation of strains and stresses using the present approach gives homogenized, continuum-level measures of the mechanical environment within the LC, rather than individual laminar beam-level strain and stress. In a preliminary report, we have demonstrated by using FE modeling that the mechanical milieu at beam-level refinement can be much more diverse than presented using the homogenized continuum approach (Kodiyalam S, et al. *IOVS* 2008;49:ARVO E-Abstract 3667).[47]

Another important limitation of the present study is that the small number of specimen-specific finite element models (three pairs) limits the study's ability to generalize regarding changes in the biomechanical environment that arise due to EG. Although each of the models reflected individualized geometric and microarchitectural features of the LC and peripapillary sclera, scleral shell thickness and scleral stiffness were derived from previously pooled data, and LC stiffness was adjusted over a range by a proportionality constant to explore biomechanical response to IOP elevation. Such a modeling approach, unfortunately, precludes us from rigorously studying the relative contribution of—and interaction between—multiple geometric and material factors via parameterized sensitivity analysis or design of experiment approaches in the manner adopted by Sigal et al.[35,36,48] for the study of ONH biomechanics. For example, we noted in two of the models (monkeys 2 and 3) that the EG eye was able to displace anteriorly at a lower LC stiffness value and displace by a greater amount than was possible for the normal eye. This may be explained in part by the fact that an LC with deeper curvature has more capacity to displace anteriorly under increased IOP than a flatter lamina. Indeed, in the normal eye of monkey 3, where the lamina was notably thinner and flatter than the other eyes, the average net anterior LC displacement was limited to a maximum of approximately 5 μm. To make more generalized statements regarding the effect on LC depth (and other factors) on LC displacement using the present modeling approach, a larger population of specimen-specific models would need to be generated and analyzed. As an alternative, a complementary parametric study of the material and geometric characteristics underlying the polarity and magnitude of LC deformation is currently under way in our laboratory and will be the subject of a separate report.

In conclusion, we have presented eye-specific FE models for three pairs of monkey eyes with unilateral early EG. Our models suggest that the LC of both normal and EG eyes has the capacity to move posteriorly or anteriorly under acute IOP elevation, depending on the material stiffness of the LC, and that scleral canal expansion is generally less in EG eyes. Whether the strain environment of the LC is similar or different between normal and EG eyes depends on the stiffness of the laminar connective tissue in the normal and EG states, with strains being higher in EG eyes when their LCs are sufficiently plaint to exhibit substantial posterior deformation. Laminar stresses were found to be consistently lower in the EG eye, regardless of the underlying material stiffness of the LC. Hence, we conclude that connective tissue remodeling in EG alters the biomechanical response of the LC to IOP elevation in an eye-specific manner. Based on two of the three monkeys, the model results suggest that the LC tissues in EG eyes are more plaint than their contralateral normal eyes. Our results highlight the importance of developing new imaging technologies to scan the deeper connective tissues of the ONH and particularly emphasize LC surface displacement and scleral canal expansion as imaging targets during acute IOP elevation experiments.

Acknowledgments

The authors thank Juan Reynaud and Jonathan Grimm for contributions to hardware and software development and Rich Hart, Anthony

Bellezza, and Budd Hirons for early iterations of the modeling approach.

References

1. Quigley HA, Addicks EM, Green WR, Maumenee AE. Optic nerve damage in human glaucoma. II. The site of injury and susceptibility to damage. *Arch Ophthalmol.* 1981;99:635–649.
2. Hernandez MR, Igoe F, Neufeld AH. Cell culture of the human lamina cribrosa. *Invest Ophthalmol Vis Sci.* 1988;29:78–89.
3. Clark AF, Browder SL, Steely HT, Wilson K, Cantu-Crouch D, McCartney MD. Cell biology of the human lamina cribrosa. In: Drance SM, Anderson DR, ed. *Optic Nerve in Glaucoma*. Amsterdam/New York: Kugler Publications; 1995:79–105.
4. Hernandez MR. The optic nerve head in glaucoma: role of astrocytes in tissue remodeling. *Prog Retin Eye Res.* 2000;19:297–321.
5. Burgoyne CF, Downs JC, Bellezza AJ, Suh JK, Hart RT. The optic nerve head as a biomechanical structure: a new paradigm for understanding the role of IOP-related stress and strain in the pathophysiology of glaucomatous optic nerve head damage. *Prog Retin Eye Res.* 2005;24:39–73.
6. Fechtner RD, Weinreb RN. Mechanisms of optic nerve damage in primary open angle glaucoma. *Surv Ophthalmol.* 1994;39:23–42.
7. Anderson DR, Drance SM, Schulzer M. Factors that predict the benefit of lowering intraocular pressure in normal tension glaucoma. *Am J Ophthalmol.* 2003;136:820–829.
8. Investigators TA. The advanced glaucoma intervention study (AGIS): 7. the relationship between control of intraocular pressure and visual field deterioration. *Am J Ophthalmol.* 2000;130:429–440.
9. Kass MA, Heuer DK, Higginbotham EJM, et al. The Ocular Hypertension Treatment Study: a randomized trial determines that topical ocular hypotensive medication delays or prevents the onset of primary open-angle glaucoma. *Arch Ophthalmol.* 2002;120:701–713.
10. Leske MC, Heijl A, Hussein M, Bengtsson B, Hyman L, Komaroff E. Factors for glaucoma progression and the effect of treatment: the early manifest glaucoma trial. *Arch Ophthalmol.* 2003;121:48–56.
11. Morrison JC, Johnson EC, Cepurna W, Jia L. Understanding mechanisms of pressure-induced optic nerve damage. *Prog Retin Eye Res.* 2005;24:217–240.
12. Roberts MD, Grau V, Grimm J, et al. Remodeling of the connective tissue microarchitecture of the lamina cribrosa in early experimental glaucoma. *Invest Ophthalmol Vis Sci.* 2009;50:681–690.
13. Yang H, Downs JC, Girkin C, et al. 3-D Histomorphometry of the normal and early glaucomatous monkey optic nerve head: lamina cribrosa and peripapillary scleral position and thickness. *Invest Ophthalmol Vis Sci.* 2007;48:4597–4607.
14. Downs JC, Roberts MD, Burgoyne CF. Mechanical environment of the optic nerve head in glaucoma. *Optom Vis Sci.* 2008;85:425–435.
15. Burgoyne CF, Downs JC. Premise and prediction-how optic nerve head biomechanics underlies the susceptibility and clinical behavior of the aged optic nerve head. *J Glaucoma.* 2008;17:318–328.
16. Roberts MD, Liang Y, Sigal IA, et al. Correlation between local stress and strain and lamina cribrosa connective tissue volume fraction in normal monkey eyes. *Invest Ophthalmol Vis Sci.* 51: 295–307.
17. Yang H, Downs JC, Sigal IA, Roberts MD, Thompson H, Burgoyne CF. Deformation of the normal monkey optic nerve head connective tissue following acute IOP elevation within 3-D histomorphometric reconstructions *Invest Ophthalmol Vis Sci.* 2009;50:5785–5799.
18. Burgoyne CF, Downs JC, Bellezza AJ, Hart RT. Three-dimensional reconstruction of normal and early glaucoma monkey optic nerve head connective tissues. *Invest Ophthalmol Vis Sci.* 2004;45: 4388–4399.
19. Downs JC, Yang H, Girkin C, et al. Three dimensional histomorphometry of the normal and early glaucomatous monkey optic nerve head: neural canal and subarachnoid space architecture. *Invest Ophthalmol Vis Sci.* 2007;48:3195–3208.
20. Yang H, Downs JC, Bellezza AJ, Thompson H, Burgoyne CF. 3-D histomorphometry of the normal and early glaucomatous monkey optic nerve head: prelaminar neural tissues and cupping. *Invest Ophthalmol Vis Sci.* 2007;48:5068–5084.
21. Grau V, Downs JC, Burgoyne CF. Segmentation of trabeculated structures using an anisotropic Markov random field: application to the study of the optic nerve head in glaucoma. *IEEE Trans Med Imaging.* 2006;25:245–255.
22. Downs JC, Blidner RA, Bellezza AJ, Thompson HW, Hart RT, Burgoyne CF. Peripapillary scleral thickness in perfusion-fixed normal monkey eyes. *Invest Ophthalmol Vis Sci.* 2002;43:2229–2235.
23. Downs JC, Ensor ME, Bellezza AJ, Thompson HW, Hart RT, Burgoyne CF. Posterior scleral thickness in perfusion-fixed normal and early-glaucoma monkey eyes. *Invest Ophthalmol Vis Sci.* 2001;42: 3202–3208.
24. Downs JC, Suh JK, Thomas KA, Bellezza AJ, Burgoyne CF, Hart RT. Viscoelastic characterization of peripapillary sclera: material properties by quadrant in rabbit and monkey eyes. *J Biomech Eng.* 2003;125:124–131.
25. Downs JC, Suh JK, Thomas KA, Bellezza AJ, Hart RT, Burgoyne CF. Viscoelastic material properties of the peripapillary sclera in normal and early-glaucoma monkey eyes. *Invest Ophthalmol Vis Sci.* 2005;46:540–546.
26. Roberts MD, Hart RT, Liang Y, Bellezza AJ, Burgoyne CF, Downs JC. *Continuum-Level Finite Element Modeling of the Optic Nerve Head Using a Fabric Tensor Based Description of the Lamina Cribrosa.* Presented at the American Society of Mechanical Engineers (ASME) Summer Bioengineering Conference. Keystone, CO; 2007.
27. Sigal IA, Flanagan JG, Tertinegg I, Ethier CR. Modeling individual-specific human optic nerve head biomechanics. Part I: IOP-induced deformations and influence of geometry. *Biomech Model Mechanobiol.* 2009;50:85–98.
28. Sigal IA, Flanagan JG, Tertinegg I, Ethier CR. Modeling individual-specific human optic nerve head biomechanics. Part II: influence of material properties. *Biomech Model Mechanobiol.* 2009;50:99–109.
29. Inoue R, Hangai M, Kotera Y, et al. Three-dimensional high-speed optical coherence tomography imaging of lamina cribrosa in glaucomax. *Ophthalmology.* 2009;116:214–222.
30. Srinivasan VJ, Adler DC, Chen Y, et al. Ultrahigh-speed optical coherence tomography for three-dimensional and en face imaging of the retina and optic nerve head. *Invest Ophthalmol Vis Sci.* 2008;49:5103–5110.
31. Fortune B, Yang H, Strouthidis NG, et al. The effect of acute intraocular pressure elevation on peripapillary retinal thickness, retinal nerve fiber layer thickness and retardance. *Invest Ophthalmol Vis Sci.* 2009;50:4719–4726.
32. Girard M, Downs JC, Burgoyne CF, Bottlang M, Suh JK. *Nonlinear Finite Element Modeling of Monkey Posterior Sclera under Intraocular Pressure*. Presented at the American Society of Mechanical Engineers (ASME) Summer Bioengineering Conference. Keystone, CO; 2007.
33. Girard MJ, Downs JC, Bottlang M, Burgoyne CF, Suh JK. Peripapillary and posterior sclera mechanics. Part II: experimental and inverse finite element characterization. *J Biomech Eng.* 2009;131: 051012.
34. Girard MJ, Suh JK, Bottlang M, Burgoyne CF, Downs JC. Scleral biomechanics in the aging monkey eye. *Invest Ophthalmol Vis Sci.* 2009;50:5226–5237.
35. Sigal IA, Flanagan JG, Ethier CR. Factors influencing optic nerve head biomechanics. *Invest Ophthalmol Vis Sci.* 2005;46:4189–4199.
36. Sigal IA. Interactions between geometry and mechanical properties on the optic nerve head. *Invest Ophthalmol Vis Sci.* 2009;50: 2785–2795.
37. Cowin SC, Doty SB. *Tissue Mechanics*. New York: Springer; 2007: 682.
38. Ethier CR, Simmons CA. *Introductory Biomechanics: From Cells to Organisms*. New York: Cambridge University Press; 2007.
39. Kirwan RP, Crean JK, Fenerty CH, Clark AF, O'Brien CJ. Effect of cyclical mechanical stretch and exogenous transforming growth factor-beta1 on matrix metalloproteinase-2 activity in lamina cri-

brosa cells from the human optic nerve head. *J Glaucoma.* 2004; 13:327–334.

40. Kirwan RP, Fenerty CH, Crean J, Wordinger RJ, Clark AF, O'Brien CJ. Influence of cyclical mechanical strain on extracellular matrix gene expression in human lamina cribrosa cells in vitro. *Mol Vis.* 2005;11:798–810.
41. Morrison JC. Integrins in the optic nerve head: potential roles in glaucomatous optic neuropathy (an American Ophthalmological Society thesis). *Trans Am Ophthalmol Soc.* 2006;104:453–477.
42. Humphrey JD. Stress, strain, and mechanotransduction in cells. *J Biomech Eng.* 2001;123:638–641.
43. Turner CH. On Wolff's law of trabecular architecture. *J Biomech.* 1992;25:1–9.
44. Gibson LJ, Ashby MF. *Cellular Solids: Structures and Properties*. 2nd ed. Cambridge University Press; 1999:532.
45. Mills N. *Polymer Foams Handbook: Engineering and Biomechanics Applications and Design Guide.* Oxford, UK: Butterworth-Heinemann; 2007.
46. Pahr DH, Zysset PK. A comparison of enhanced continuum FE with micro FE models of human vertebral bodies. *J Biomech.* 2009;42:455–462.
47. Downs J, Roberts MD, Burgoyne CF, Hart RT. Multiscale finite element modeling of the lamina cribrosa microarchitecture in the eye. *Conf Proc IEEE Eng Med Biol Soc.* 2009;1:4277–4280.
48. Sigal IA, Flanagan JG, Tertinegg I, Ethier CR. Finite element modeling of optic nerve head biomechanics. *Invest Ophthalmol Vis Sci.* 2004;45:4378–4387.